Electrodeposition of manganese layers from sustainable sulfate based electrolytes

Mónica Fernández-Barcia*, Volker Hoffmann, Steffen Oswald, Lars Giebeler, Ulrike Wolff, Margitta Uhlemann, Annett Gebert

IFW Dresden, Institute for Complex Materials, Helmholtzstraße 20, 01069 Dresden, Germany

Keywords: Mn electrodeposition, pH control, Sustainable electrolyte, $(NH_4)_2SO_4$, GD-OES, XPS

A B S T R A C T

Functional manganese-(Mn)-containing layers are becoming increasingly important in the fields of sacrificial corrosion protection, biodegradable medical devices or electrochemical energy conversion systems. Electrodeposition can be a low cost and time-efficient production route, but the very electronegative nature of Mn makes this reduction process quite challenging.
In this paper, electrolytic potentiostatic deposition of metallic Mn layers from environmentally friendly aqueous manganese sulfate electrolytes with pH 3 is successfully demonstrated. A continuous electrolyte flow in the cathodic compartment of the electrochemical cell for controlling the pH value during deposition was found to be essential for achieving good layer qualities. Based on cyclic voltammetry analysis in combination with quartz crystal microbalance measurements a suitable deposition potential range was identified. The obtained electrodeposited layers were characterized by means of SEM, XRD, GD-OES and XPS. The shift of the deposition potential from −2.4 V_{MSE} to −2.6 V_{MSE} (deposition time 60 min) yields a thickness increase of the metallic α-Mn deposits from< 500 nm to ∼2 μm. Only thin additional surface regions of Mn-oxides/-hydroxides were identified. The important role of $(NH_4)_2SO_4$ as complex-forming electrolyte additive is discussed and an impact of the salt concentration on the deposit properties is revealed. This is a promising starting point for further Mn alloy deposition analysis.

1. Introduction

Metallic manganese (Mn) and its alloys have attracted the attention of research on coatings for steel products since almost a century, due to their combination of good sacrificial corrosion protection and suitable mechanical properties [1,2]. Recently, Mn became also in the focus as constituent of biodegradable Fe-based alloys and it has been found to support a good balance between corrosive degradation and mechanical integrity, which is necessary for implant applications [3,4,5]. Accordingly, Mn-containing compounds are considered as interesting new materials for parts of biodegradable electronic devices, as e.g. thin electrodes or packaging layers [6]. Due to their thermodynamic and electrochemical properties, Mn and its oxidized compounds have been proposed as good candidates for electrode materials of batteries and supercapacitors [7]. From these perspective application fields derives the need to develop suitable, low cost and environmentally sustainable preparation routes for Mn and Mn-containing layers and microstructures. Electrodeposition is a promising approach, which can meet these requirements. Mn has a very low standard electrode potential of $E_{Mn^{2+}/Mn}$ = −1.83 V_{MSE}, which makes Mn the most electronegative

metal that can be electrodeposited from aqueous solutions.
Nowadays, the integration of sustainability in technological progress is becoming one of the most important challenges in the modern society. Additives as Se or Te compounds to water-based electrolytes have been used to decrease the hydrogen evolution reaction, HER, and to improve the properties of the electrodeposited Mn layers [8,9]. However, these compounds must be avoided due to the toxicity and hazard that they present for the environment and the contamination of the resulting Mn layers. Further, organic electrolytes could be chosen as base electrolyte in order to avoid the decomposition of the electrolyte but they generate problematic waste. For this reason, water should be selected as standard base electrolyte despite its limited potential window of stability. Even though Mn can be electrodeposited from acidic sulfate and chloride baths, chloride baths showed a better efficiency [10]. However, a sulfate bath should be chosen in order to avoid the negative impact provided by the chloride medium, e.g. the corrosive nature of the solution and Cl_2 formation [11].
As it was previously mentioned, Mn layers can be electrodeposited from acidic sulfate and chloride baths, but only together with corresponding ammonium salts [2,10,12,13], which are essential for the growth of Mn coatings with good coverage. Ammonium salts such as ammonium sulfate, $(NH_4)_2SO_4$, not only support the formation of dense and adhesive layers, but also present some other advantages. The precipitation of manganese hydroxides during the electrodeposition process is partially inhibited through a preferential ammonium complex formation. In aqueous electrolytes containing $MnSO_4$ and $(NH_4)_2SO_4$, Mn^{2+} ions can form different complexes: $[Mn(H_2O)_6]^{2+}$, $[Mn(NH_3)_{x = 1–6}]^{2+}$ or $[Mn(H_2O)_{6-n}(NH_3)_n]^{2+}$. It has been proposed that Mn^{2+} could be discharged by those complexes present in the electrolyte, increasing the Mn^{2+} ion discharge ability [1,14]. Also, $(NH_4)_2SO_4$ has a buffering effect at pH values between 2 and 3.5 as well as between 6 and 7, which stabilize the pH value near the cathode surface to this limited extent. $(NH_4)_2SO_4$ as a supporting salt in the electrolyte causes an improvement of the conductivity of the electrolyte. Nevertheless, as reported in literature [1,15], even when $(NH_4)_2SO_4$ was used, the chemical analysis of the electrodeposited layers always revealed besides metallic Mn the presence of oxides and hydroxides on the surface or its core. In addition, the advantages provided by the addition of the $(NH_4)_2SO_4$ are counteracted by a decrease in the overpotential for HER, which is a common side reaction and reduces the current efficiency of the electrodeposition process.
Boric acid, H_3BO_3, has not been commonly used in the Mn electrodeposition process reported by previous authors. When the presence of H_3BO_3 in the bath was reported, its action as a buffer agent was

implied without further information [10]. Nevertheless, H_3BO_3 is often used in Ni or Fe electrodeposition improving the quality of the deposits. Generally, the exact mechanism of role of H_3BO_3 is not well understood and some explanations have been considered: (1) H_3BO_3 acts as a buffer, (2) it adsorbs on the electrode surface blocking the active place for hydrogen evolution and (3) it forms complexes with the metal ions [16,17]. However, later studies as numerical simulations and experiments conducted by Zech and Landolt [18] have proved that the presence of H_3BO_3 retards the increase of the pH value at the cathode surface. This is explained by a release of protons in the cathodic diffusion layer at potential values where water reduction starts to be possible. Those facts are attributed to the adsorption of the H_3BO_3 species to the surface [18]. Due to its effect on the pH value at the cathode surface, H_3BO_3 was included as a component of the bath in the present study. More recent studies in Ni electrodeposition have attributed to the H_3BO_3 a capping effect due to the inhibition of the crystal growth along a specific orientation, which takes place by the adsorption of the H_3BO_3 onto specific crystal face [19].
The aim of this work is to develop a Mn electrodeposition process from sustainable water-based sulfate and ammonium electrolytes, with minimum amounts of scarce, toxic or high concern substances. Electrodeposition is conducted under potentiostatic control and a special focus is set on the effect of the applied potential and of the $(NH_4)_2SO_4$ concentration on the morphology of the generated layers as well as on their chemical composition and thickness. Long deposition times have to be applied to obtain thicker layers, whereby a significant increase of the pH value of the electrolyte was revealed. This behavior triggers the formation of manganese hydroxides. The control and adjustment of the pH value of the electrolyte bath during the deposition process was identified to be essential for the preparation of metallic Mn layers with good quality.

2. Materials and methods

The electrodeposition experiments were carried out in a threeelectrode, two-compartment Teflon® cell without and with electrolyte flow in the cathodic compartment. The electrolyte flow system consists in a closed circuit between the cathodic compartment of the electrochemical cell and an external reservoir. A pH-meter and a stirring bar are placed in the external reservoir, which only contains the electrolytic bath. In this manner, the pH value is controlled and adjusted before and during the electrodeposition process. Furthermore, the closed circuit allows to use a minimum quantity, i.e. 60 mL, of electrolyte for each electrodeposited Mn layer. Consequently, by reducing the quantity of the electrolyte, a lower quantity of waste is generated, paving the way

for a sustainable process in addition to a sustainable electrolyte. A flow velocity of 5 mL/min was optimized and realized with a peristaltic pump (Ismatec® MS-CA 4/640), in order to maintain the bulk pH value constant during the time of the electrodeposition. Layers have been electrodeposited on polycrystalline Au layers sputtered (200 nm) on glass and Si wafers with an area equal to 0.785 cm^2 which were arranged horizontally in the bottom of the cell. The counter electrode was a platinum coil included in the anodic compartment. It was separated from the cathodic compartment by a NAFION membrane (Nafion® N-115 membrane, 0.125 mm thick, ≥0.90 meq/g exchange capacity, Alfa Aesar) to avoid the oxidation of Mn^{2+} ions in the electrolytic bath and, in this way, to avoid the formation of other solid compounds (oxides or hydroxides) which could be incorporated into the deposits. All potentials were measured vs. mercury-mercurous sulfate electrode (MSE, E_{SHE} = 0.650 V) as reference electrode. This electrode was located in an external compartment and connected to the cell by a Luggin capillary. For standard test this cell was connected to an IPS-300 mA-10 V potentiostat. Also, electrochemical quartz crystal microbalance (EQCM, Quartz Crystal Analyzer QCA922, SEIKO EG&G) measurements were conducted. For the EQCM the cell was modified; a mirror finished sputtered gold layer, with an area of 0.196 cm^2 and roughness of 0.06 μm, on top of a quartz crystal was used as a working electrode. The sensitivity factor for the used quartz crystal is 0.21 $Hz \cdot cm^2/g$ at room temperature. The electrochemical cell was connected to a BioLogic SP-200.

EQCM measurements are based on the fact that quartz crystals possess through the piezo-electric effect a resonance frequency

$$f_0 = \frac{1}{2d}\left(\frac{\mu_c}{\rho_c}\right)^{1/2} \quad (1)$$

where f_0 is the resonance frequency, μ_c is the shear modulus, ρ_c is the density, and d is the thickness: constant parameters of the quartz. The EQCM signal was registered as Δf_{exp} (Hz) (=$f-f_0$), an indirect measurement of the change of mass: increases in weight give rise to decreases in frequency, explained by the Sauerbrey equation

$$\Delta f = -(2f_0^2/(\mu_c\rho_c)^{1/2})\Delta m \quad (2)$$

Δm represents the total mass change per square cm which occurs at the electrode surface, which corresponds to the mass change due to the deposition and dissolution of the metal, and the contributions from adsorbed and trapped solvent molecules [20].

The two electrolytes used in the present work contained 0.05 M $MnSO_4 \cdot H_2O$ (Merck KGaA) as source of Mn^{2+}, 0.5 M or 1 M $(NH_4)_2SO_4$

as supporting electrolyte and complexing agent (Emsure® analysis grade) and 0.3 M H_3BO_3 (Merck KGaA, analysis grade) as an additional buffer and to release the internal stress. Different to the most of the previous studies, H_3BO_3 was used but in low concentration since it is necessary to be aware due to its placement as a candidate in the list of "substances of high concern". Therefore, it cannot be present in the final layers in a concentration higher than 5.5% [21]. The pH value of the initial electrolyte and later, during the electrodeposition process was adjusted to 3 with 0.5 M H_2SO_4.

Cyclic voltammetry experiments were performed at a sweep rate of 20 mV/s. The potential steps was firstly scanned from the open circuit potential (OCP) in negative direction to −3.0 V_{MSE} and then reversed. From pre-experimental cyclic voltammograms and EQCM measurements, potentials for the potentiostatic experiments were chosen: -2.4 V, −2.5 V and −2.6 V (vs. MSE). These electrodeposition experiments were carried out at room temperature for 60 min.

The morphology of the deposits was characterized with scanning electron microscopy (SEM, Leo Gimini 1530, Zeiss/XFlash4010, Bruker) coupled with energy dispersive X-ray spectroscopy (EDX). The chemical composition of the samples was analyzed by means of the glow discharge optical emission spectrometry (GD-OES) depth profiling technique. A radio-frequency (rf) source designed and built in-house was employed to produce sputtering craters of 2.5 mm in diameter. The construction is based on the Universal Sample Unit from Spectruma Analytik GmbH, where the sputtering source is sealed by a cup and not by the rough and porous sample itself. Discharge parameters of 600 V anode voltage, 197 Hz, a duty cycle of 10% and 4.2 hPa Ar pressure were used for the analysis of the synthesized samples. These conditions resulted in a sufficiently flat crater shape and an erosion rate 12 nm/s for the metallic Mn. Intensity-time curves of selected emission lines O 130 nm, Mn 403 nm, Au 479, B 208 nm and Si 288 nm were recorded using a high sensitive Photomultiplier (PMT) based GDA750 (Spectruma Analytik GmbH) [22,23]. Calibration of the signal was not done and the signal intensity obtained is not directly related with the atomic concentration of the considered elements. X-ray photoelectron spectroscopy (XPS, PHI 5600, Physical electronics) was used to characterize the chemical surface state of the electrodeposited layers. These measurements were carried out with a PHI 5600CI (Physical Electronics) spectrometer, which is equipped with a hemispherical analyzer running at a typical pass energies of 90 eV for survey and of 29 eV for detailed spectra. The analysis area was around 800 μm in diameter. Monochromatic Al-Kα excitation (350 W) was used. Depth profiling was performed using Ar^+ ions at an acceleration voltage of 3.5 keV with an abrasion of 3.3 nm/min on SiO_2. XRD patterns were recorded on a STOE Stadi P diffractometer with a curved Ge (111) crystal as

primary beam monochromator for Mo $K\alpha_1$ radiation and a Mythen 1 K position sensitive detector (Dectris). All deposited materials on the substrates were measured as flat samples in transmission geometry as prepared.

3. Results and discussion

3.1. Electrochemical studies

In order to characterize the cathodic reduction reactions in a Mn^{2+} containing electrolyte: 0.05 M $MnSO_4$, 0.3 M H_3BO_3 and 1 M $(NH_4)_2SO_4$ more in detail, potentiodynamic polarization studies (cyclic voltammograms, CV) in combination with electrochemical quartz crystal microbalance (EQCM) measurements were performed under electrolyte flow conditions in the cathodic compartment. By means of the mass change of the EQCM, it is possible to distinguish between the Mn reduction and the side reactions which are not related with mass change.

Fig. 1 shows a CV recorded together with the corresponding mass change curve which was obtained from the Δf_{exp} measurements of the EQCM after application of the Sauerbrey equation (Eq. (2)). From a starting value of−0.25 V_{MSE} (OCP, open circuit potential) the potential was scanned in negative direction up to an end value of −3.0 V_{MSE}. From a potential of −1.6 V_{MSE} (I) the cathodic current density gradually increases but with no significant change in the corresponding mass curve. However, from −2.1 V_{MSE} (II) the slope of the current density-potential curve increases which is related to an increase in the mass change curve. These features indicate the beginning of the Mn^{2+} reduction and deposition. At this negative potential range, the metal ion reduction is superimposed by the HER which contributes to the total current density response, but no to the mass change. In the reverse scan, a deviation in the current density curve shape begins at −1.98 V_{MSE} (III) and develops to a characteristic anodic peak with maximum at −1.75 V_{MSE} (IV). This is accompanied with a peak in the mass change curve, which corresponds to the loss of mass indicating the oxidation of Mn deposits and dissolution. From the analysis of those cyclic polarization studies, a suitable potential range for the following potentiostatic deposition experiments was derived from −2.4 to −2.6 V_{MSE}.

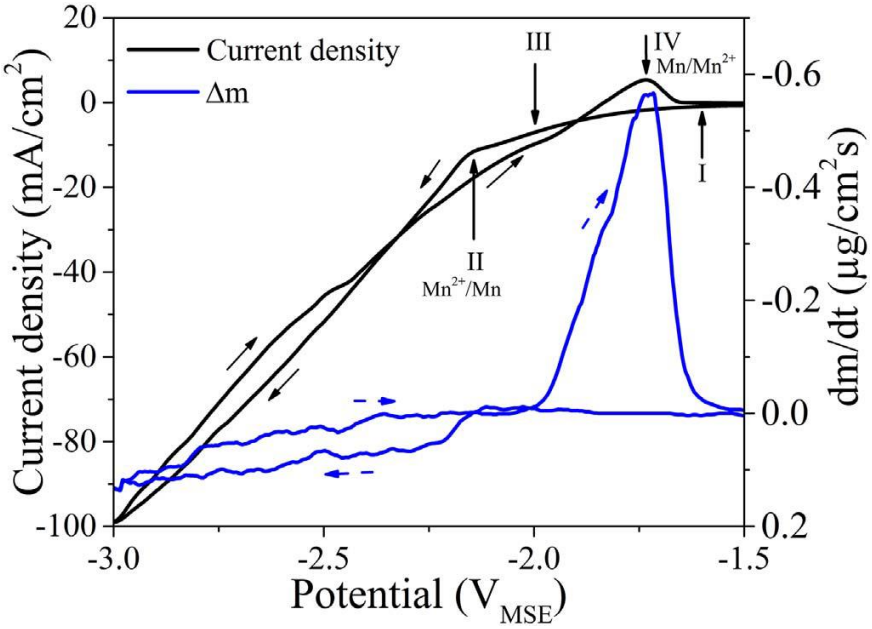

Fig. 1. Cyclic voltammogram and corresponding mass change curve measured in the electrolyte containing 0.05 M $MnSO_4$, 1 M $(NH_4)_2SO_4$ and 0.3 M H_3BO_3 under electrolyte flow. Scan rate 20 mV/s.

3.2. Effect of the electrolyte flow

A first series of electrodeposition experiments was conducted at −2.4 V_{MSE} and −2.6 V_{MSE} for 60 min, the two extremes of the potential range chosen in the two compartment cell only under natural electrolyte convection. Additional potentiostatic tests were realized at −2.6 V_{MSE} for 60 min under electrolyte flow in the cathodic compartment. The pH value in the cathodic compartment was measured during all the experiments, as shown in Fig. 2.

Without flow already within the first minutes of deposition the pH value increases from 3 to 6 and upon prolonged deposition the pH value rises more gradually up to 9. The more negative the applied potential, the faster is the increase of the pH value. At these potentials the HER superimposes as side reaction of Mn^{2+} reduction and causes therefore, a strong increase of the pH value in the vicinity of the cathode surface and then, of the bulk electrolyte.

In such an environment only $Mn(OH)_2$ deposits can be expected. Exemplarity, electrolyte flow conditions were realized for deposition at −2.6 V_{MSE} and adjust to 5 mL/s. In this case, the pH value curve in Fig. 2 demonstrates the perfect maintenance of a pH~3, which was suggested as optimum condition for Mn deposition [1]. Consequently,

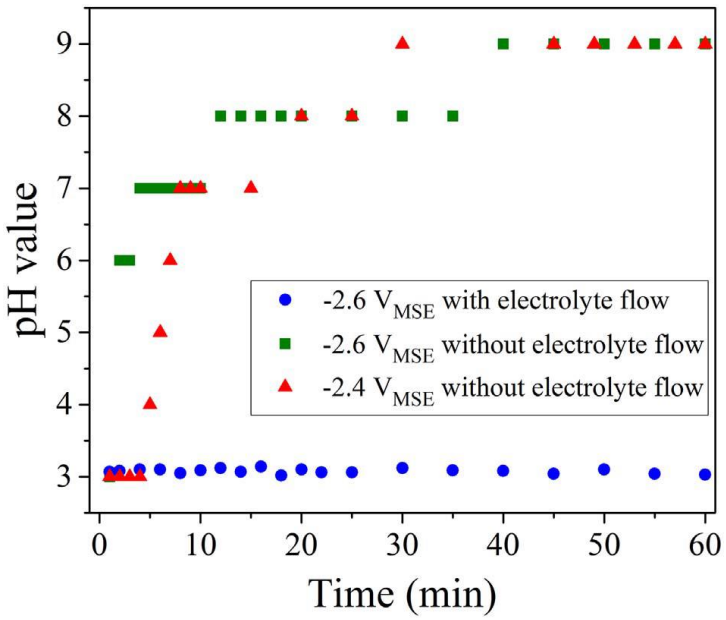

Fig. 2. Change of the pH value of electrolyte in the cathodic compartment during the electrodeposition studies in the electrolyte containing 0.05 M $MnSO_4$, 1 M $(NH_4)_2SO_4$ and 0.3 M H_3BO_3. Electrolyte flow: 5 mL/s.

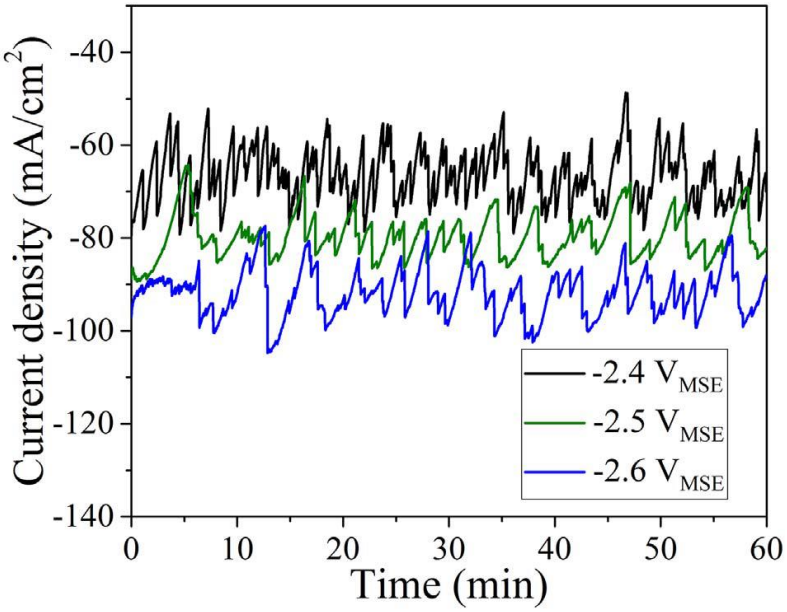

Fig. 3. Current density-time transient curves at different applied potential values in electrolyte containing 0.05 M $MnSO_4$, 1 M $(NH_4)_2SO_4$ and 0.3 M H_3BO_3 without electrolyte flow.

further deposition experiments were performed always with electrolyte flow.

Fig. 3 shows the current density-time transient curves measured at the three chosen applied potentials for potentiostatic experiments. These curves reflect how current density increase by increasing the applied potential, in a range between −60 and −100 mA/cm2. It is

also reflected periodic fluctuations, which belong to the evolution of hydrogen bubbles. These fluctuations remain even when electrolyte flow is applied in the cathodic compartment.
Due to the very negative potential region, where the Mn^{2+} reduction takes places, the iR drop must be considered in the polarization measurement. It might change the sweep rate and have an impact in the slope of the potentiodynamic polarization studies. The iR drop was estimated using the formula

$$R = [\arctan(z/r)]/2\pi\kappa r \quad (3)$$

where R is the resistance of the electrolyte at a circular working electrode, r is the radius of the circular working electrode (5 mm), z is the distance between the working electrode and the tip of the Luggin capillary (12.63 mm) and κ is the specific conductivity of the electrolyte solution (77 $m\Omega \cdot cm^{-1}$) [24]. For the given experimental conditions R =0.28 mΩ was estimated. At the chosen applied potentials, the current density fluctuates between −60 and −100 mA/cm^2 (Fig. 3). This corresponds to iR drop values between 13 and 22 mV, which can be considered negligible and no effect was observed in potentiodynamic polarization or potentiostatic studies. Throughout the paper, all the potential values correspond to the applied potential.

3.3. Chemical and morphological characterization

The analysis of the morphology of the deposits obtained from potentiostatic experiments was performed by SEM. No clear effect of the applied potential on the surface morphology was revealed, as obvious from the top view images in the insets of Fig. 4. In all cases a porous and inhomogeneous surface was observed. However, the cross-section analysis of the deposits provided deeper information on the bulk of the layer, as shown in Fig. 4. Two regions with significantly different morphologies were detected: a porous layer on top (region A) and a thicker dense layer directly formed onto the gold layer of the substrate (region B).
EDX analysis confirmed the presence of manganese and oxygen species (not shown in this paper). A more detailed chemical analysis of the electrodeposits was possible by means of GD-OES. Depth profiles of deposits obtained at −2.4, −2.5 and 2.6 V_{MSE} are shown in Fig. 5 as plots of the relative intensities of the element signals versus the sputtering time. In all depth profiles two regions of the deposits are identifiable, i.e. an oxygen rich outer layer and a main inner layer, mostly composed of Mn. The principal composition was very similar for all of them, but a broader range of constant relative intensity of the Mn signal within the depth profile was only observed for the films deposited at −2.5 and −2.6 V_{MSE}, Fig. 5b and c.
In agreement with SEM cross section analysis, GD-OES depth profiles also reveal that thicker layers were obtained, when the more negative

potentials of −2.5 and −2.6 V_{MSE} were applied. Sputtering rate of 12 nm/s was calculated using a massive metallic Mn material, which permits to convert the sputtering time in sputtered depth. However, this transformation is only valid for the deposit region of pure Mn. The unknown exact composition and density of the top layer does not allow to apply the sputter rate to this region [22]. The calculated layer thickness values for the Mn regions are added to the plots in Fig. 5 and indicate a thickness increase from ~500 nm to ~2 μm with negative potential shift.

In order to clarify the nature of the oxygen-rich outer layer of the deposits, depth profiling analysis was done by means of XPS. Fig. 6 shows XPS detailed spectra of the Mn2p and O1s at different sputter depths measured for a deposit that was produced at −2.6 V_{MSE}. The O1s spectrum could be deconvoluted into three constituents corresponding to different oxygen-containing chemical bonds: water molecule (HeOeH) at 531.8–532.8 eV, hydroxide (MneOeH) at 532.5–531.5 eV and oxide (MneOeMn) at 529.3–530.0 eV [25]. However, in the present spectra only hydroxide and oxide were present; the contribution of the chemical bond in the water molecule was very low that it was not taken into consideration. In the O1s spectrum measured on the non-sputtered deposit surface, a characteristic peak corresponding to hydroxide (MneOeH) at 531.8 eV with a smooth shoulder around a value of 530 eV which corresponds to the oxide (OeMneO bond) were identified. In parallel, the Mn2p spectrum, two peaks centered at the values of 642.2 eV and 654.07 eV confirm the presence of mainly Mn oxy-hydroxide (MnO(OH)) and Mn oxides (MnO_2) [26,27]. After a first sputter step (50 nm depth), the O1s and Mn2p peaks shifted to lower binding energies, centered at 530.0 eV and 653.2 & 641.3 eV respectively. This shifting indicates that below the surface the Mn hydroxides start to disappear and a different Mn oxide in form of MnO is identified. In addition, after the first sputter step a strong change in the O1s peak and, in parallel, a small shift in Mn2p peak around the value of 641 eV and 653.2 eV can be observed. This points to a conversion from MnO_2 at the outer surface to MnO, which could be forced by the Ar^+ sputtering and the high reactivity of Mn. At a sputter depth of 100 nm or more, emergence of the peaks related to the metallic Mn, Mn(0), at binding energy values of 638.9 and 650 eV occurred (whereby the metal:oxide peak height ratio increased with sputter depth). Also, a broad peak can be distinguished around the value of ~658 eV which may correspond to MnO (oxidation state of Mn (II)) or may correspond to a satellite peak of the peak appearing at 650 eV. However, in previous studies authors have analyzed in detail the Mn oxidation states using the Mn2p lines because they are the most intense lines and they are not susceptible to potential interferences from other species. But the results have not been accurate due to the proximity

between the values of the binding energy for the different oxidation states of Mn. Despite this limitation and considering that the used energy in the present analysis was not high enough to resolve the peaks, it can be suggested that the surface of the Mn layer is mostly composed of species in states of Mn(III) and Mn(IV), which convert to Mn(II) state after sputter depths of 50 nm or more. At the same time Mn in metallic form, Mn(0), appears.
XPS results are in good agreement with the results obtained by GDOES, which confirms a high purity of the deposits for those synthesized in the bath with 1 M $(NH_4)_2SO_4$.
These results of surface analytical studies demonstrate that electrodeposition of Mn layers from an aqueous ammonium-sulfate bath

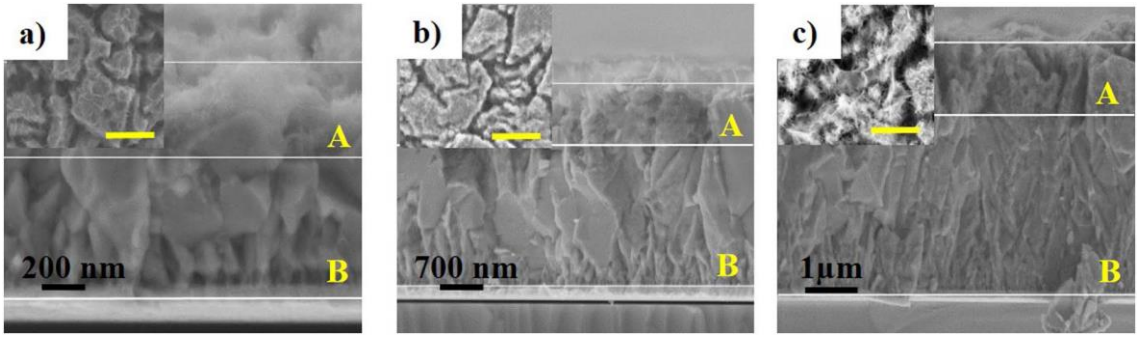

Fig. 4. SEM cross section images of Mn layers deposited at a)−2.4 V_{MSE} b)−2.5 V_{MSE} and c)−2.6 V_{MSE}. The three SEM images are accompanied by an inset showing the top view of the deposits, in which the yellow bar correspond to 1 µm. Region A: porous layer on top; and region B: dense layer. (Electrolyte composition: 0.05 M $MnSO_4$, 1 M $(NH_4)_2SO_4$ and 0.3 M H_3BO_3).

under flow conditions of the electrolyte with a pH value ~3 constant is possible. SEM and GD-OES depth profile analyses demonstrate that the thickness of the metallic layer is controlled by the applied potential. However, an outer oxidized layer region is always present. The SEM cross-section shows a porous layers only on top of the films and GD-OES depth profiling does not identify oxygen inside of the layer. It is reasonable to attribute the formation of the porous layer to the fast oxidation of the material in particular in the last period of the experiment when the applied potential is switched off and the electrode remains in the electrolyte under open circuit conditions; rather than hydroxide precipitation to occur since the bath has a constant pH value of 3. To form Mn hydroxides a pH value higher than 8 is necessary as derived from the Pourbaix diagram in Ref. [7]. On further experiments, strategies have to be developed to minimize this effect.

3.4. Effect of ammonium sulfate, $(NH_4)_2SO_4$, concentration

In order to assess the effect of the $(NH_4)_2SO_4$ concentration, the previous electrolyte with 1 M and a second electrolyte with 0.5 M of $(NH_4)_2SO_4$) were chosen. The concentration of $MnSO_4$ and H_3BO_3 remained equal to the previous experiments. Deposits were potentiostatically deposited at −2.6 V_{MSE} for 60 min under electrolyte flow conditions. The analysis of the surface morphology of the deposits was performed by SEM and an evident effect on the roughness was revealed. Deposits obtained in the electrolyte with 0.5 M $(NH_4)_2SO_4$ were generally smoother, see Fig. 7. However, deposits synthesized at both concentrations of $(NH_4)_2SO_4$ show the typical surface morphology of Mn oxides in form of needles, as indicated by arrows in Fig. 7 [28]. Principally, the $(NH_4)_2SO_4$ addition was found to be essential to achieve a good quality and coverage of the deposits from manganesesulfate bath [1]. But further, from Fig. 7 it is obvious that the concentration of this salt in the electrolyte has a significant effect on the roughness of the surface of the deposits. A roughness increase can be attributed to an enhancement of the HER which is caused by an increase of the concentration of $(NH_4)_2SO_4$. This was confirmed by potentiodynamic polarization studies. Fig. 8 shows the cathodic branches of potentiodynamic polarization curves recorded in the electrolytes with 0.5 M and 1 M of $(NH_4)_2SO_4$ in a potential range between −1.4 V and −2.1 V_{MSE}, see also Fig. 1. In this region, only the HER occurs and the significant difference between the two slopes is evident. A more pronounced rise of the cathodic current density occurs in the electrolyte with 1 M $(NH_4)_2SO_4$. Therefore, an increase of $(NH_4)_2SO_4$ concentration decreases the overpotential for HER and it triggers a higher rate of HER.

Also for the deposits, which were potentiostatically generated in this part of the study, EDX analysis confirmed the presence of manganese and oxygen species. To obtain deeper information about the chemistry of the deposits, chemical analysis was performed by means of GD-OES. Fig. 5c showed already the depth profile analysis of the deposit synthesized at −2.6 V_{MSE} in the electrolyte containing 1 M $(NH_4)_2SO_4$ which is considered here as reference state. On comparison, the depth profile obtained for the layer which was synthesized in the electrolyte with 0.5 M $(NH_4)_2SO_4$ revealed a much thinner Mn film, i.e. only 700 nm instead of 2 μm, which is again derived from the profile region where the Mn signal intensity is constant. This fact confirms that $(NH_4)_2SO_4$ enhances the Mn^{2+} ion discharge ability as it was proposed in previous studies [1]. This is the more pronounced, the higher the salt concentration is. However, in the GD-OES depth profile of the layers synthesized in the electrolyte with lower concentration of $(NH_4)_2SO_4$, also a strong signal of boron (B) appears, which its presence is also

confirmed by XPS analysis (not shown in this paper). The signal is stronger at the surface, decreases along the metallic Mn region and disappears when the sputtering process almost reaches the substrate. The lower ammonium salt concentration used is very close to the

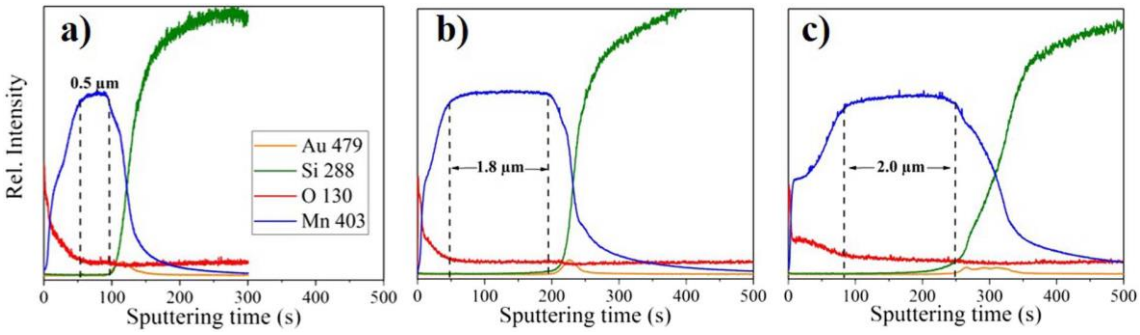

Fig. 5. GD-OES depth profile of layers deposited at a) −2.4 VMSE b) −2.5 VMSE and c) −2.6 VMSE in 0.05 M $MnSO_4$, 1 M $(NH_4)_2SO_4$ and 0.3 M H_3BO_3 electrolyte under electrolyte flow (Mn 403 nm, emission line).

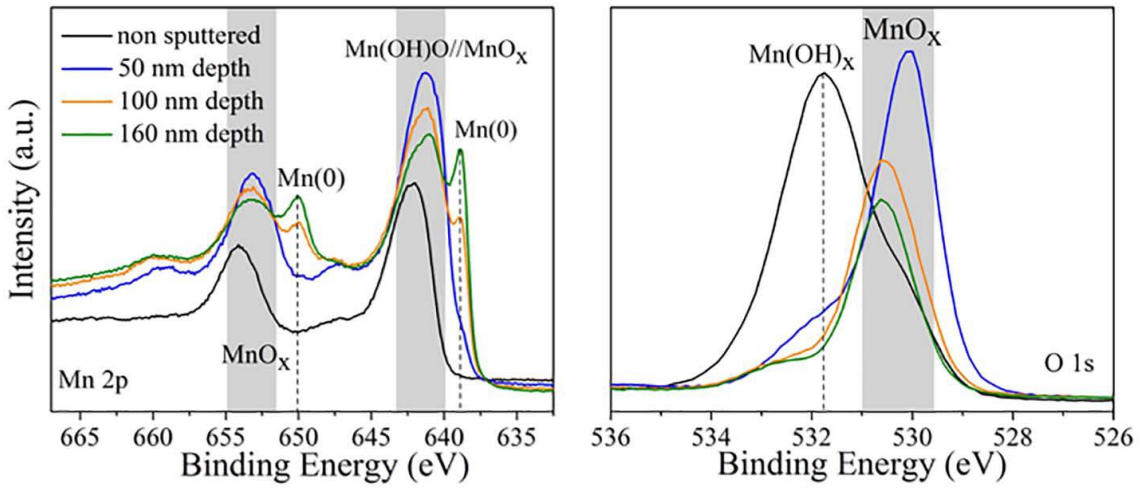

Fig. 6. XPS spectra of Mn 2p (left) and O 1 s (right) of a Mn layer electrodeposited at −2.6 VMSE in 0.05 M $MnSO_4$, 1M$(NH_4)_2SO_4$ and 0.3 M H_3BO_3 electrolyte under electrolyte flow.

concentration of H_3BO_3. This condition could allow that the H_3BO_3 takes a more important role in the electrodeposition process. In previous studies about other systems, as mentioned in the introduction, H_3BO_3 can be adsorbed at the cathode surface or in specific crystal orientation of the electrodeposited material. It can be suggested that similar events occur in the present system and that they may be the reason of the presence of B at the surface and inside of the Mn layer. However, it cannot be confirmed in this study and further experiments need to be developed.

The presence of boron reduces the purity of the Mn layers and may be the reason of the more inhomogeneous films obtained. In addition, the presence of B in the final Mn layers does not follow the restriction to develop a sustainable deposition route for Mn films.
Moreover, the crystallographic structure of the Mn layers prepared at different concentrations of $(NH_4)_2SO_4$ was studied by XRD and the obtained patterns are shown in Fig. 9. Apart from the background and reflections originating from the substrate (Si glass and Au), the other reflections are indexed by an α-Mn structure type model space group I43m, assigned to the structure model published by Bradley and Thewlis [29]. However, only the 411 main reflection with very small intensity was found from the Mn layer deposited in the electrolyte with 0.5 M $(NH_4)_2SO_4$. This observation suggests that the deposits synthesized with 0.5 M $(NH_4)_2SO_4$ electrolyte are not only morphologically refined but are also mainly amorphous or nanocrystalline. This behavior should be explained together with GD-OES results. The small intensity of the main reflection may be a consequence of the thinner thickness of the layer,

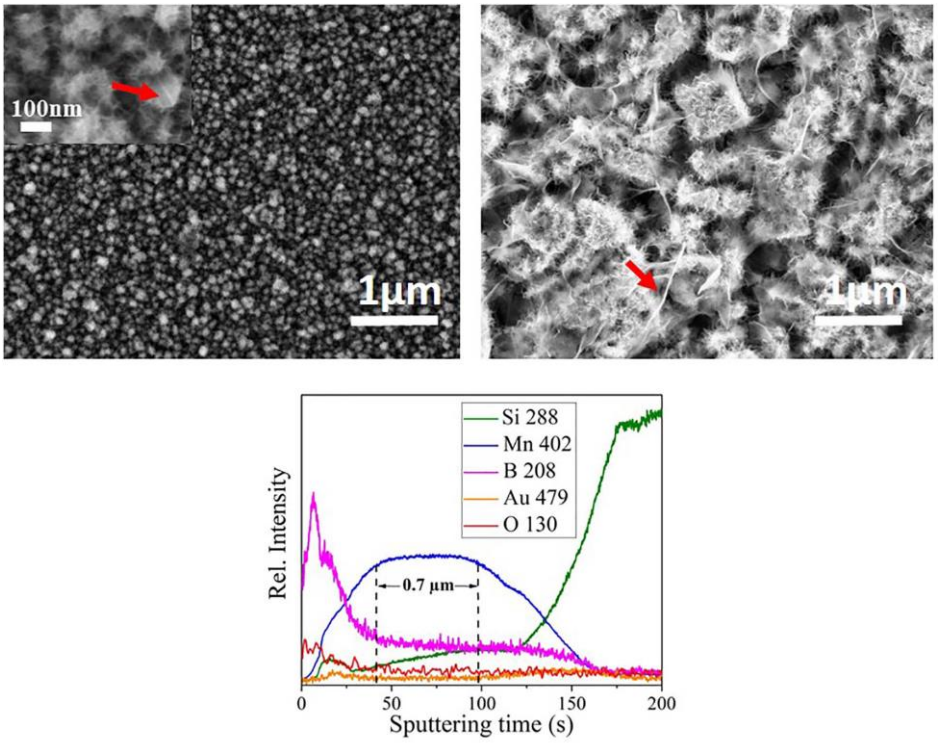

Fig. 7. SEM surface images of Mn layers deposited at 0.5 M (left) and 1 M (right) $(NH_4)_2SO_4$; GD-OES depth profile of a layer deposited at −2.6 V_{MSE} in the electrolyte with 0.5 M $(NH_4)_2SO_4$ (0.05 M $MnSO_4$, H_3BO_3) under electrolyte flow.

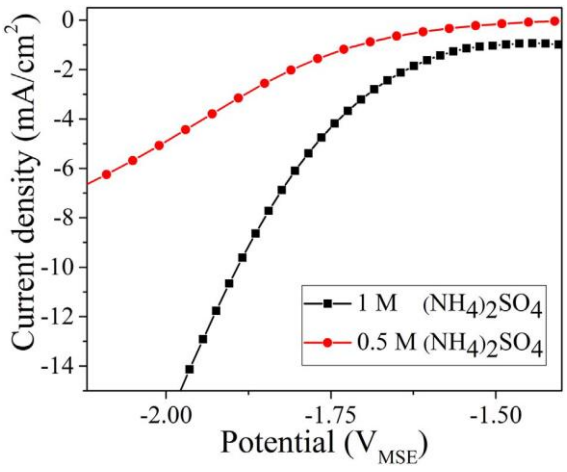

Fig. 8. Cathodic branches of potentiodynamic polarization curves recorded in the electrolytes with 1 M or 0.5 M $(NH_4)_2SO_4$ (0.05 M $MnSO_4$, 0.3 M H_3BO_3) under flow conditions. Scan rate 20 mV/s.

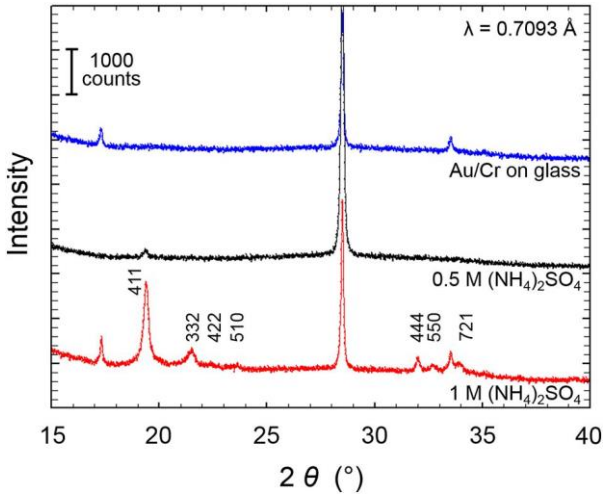

Fig. 9. XRD pattern of Mn deposits synthesized at −2.6 V_{MSE} in an electrolyte containing 0.5 M (black line) and 1 M (red line) $(NH_4)_2SO_4$, 0.05 $MnSO_4$ and 0.3 M H_3BO_3 indexed with the visible reflections of the I-43m structure type Mn.

700 nm measured by GD-OES, but also a consequence of the presence of B into the layer, which makes it amorphous. On the other hand, previous studies have investigated the phase transformation of electrodeposited Mn. A complete transformation, from γ-Mn (bct) to a more stable α-Mn (bcc) was observed in a time trace of 14 days, whereby kinetic follows the Johson-Mehl-Avrami Eq. (1). However, XRD analysis of the freshly electrodeposited Mn samples synthesized in this study revealed already the stable structure of α-Mn. The higher stability of the α-Mn yields higher values of microhardness of the electrodeposited Mn layers [1]. This could be beneficial with view to a higher mechanical integrity of those layers when used as parts of biodegradable electronic devices.

Altogether, the concentration of $(NH_4)_2SO_4$ in the electrolyte has a strong impact on the deposited Mn layers. A reduced concentration of 0.5 M $(NH_4)_2SO_4$ leads to a smoother surface and much lower thickness of the fine crystalline Mn deposits and also to a significant B contamination. However, 1 M $(NH_4)_2SO_4$ containing electrolytes lead to a constant Mn content without impurities in the deposits, a thicker thickness and a better crystallinity of the films.

4. Conclusion

Electrolytic potentiostatic deposition of metallic Mn layers from environmentally friendly aqueous manganese sulfate electrolytes with pH 3 was successfully demonstrated. The realization of a continuous electrolyte flow in the cathodic compartment of the cell for controlling the pH value during deposition at quite negative potentials was found to be essential for achieving good layer qualities. Shifting the deposition potential from −2.4 V_{MSE} to −2.6 V_{MSE} yields a remarkable thickness increase of the metallic Mn deposits. The important role of $(NH_4)_2SO_4$ addition was discussed and an impact of the salt concentration towards on the morphology, chemical composition, and structure refinement of the Mn deposits was revealed. These finding are the starting point for further Mn alloys deposition.

Acknowledgements

The authors thank K. Hennig and T. Sieger for technical support. Funding of this work by the European Commission within the H2020-MSCA-ITN-2014 SELECTA, grant agreement no. 642642 is gratefully acknowledged.

References

[1] G. Zangari, J. Gong, Electrodeposition and characterization of manganese coatings, J. Electrochem. Soc. 149 (2002) C209–C217.
[2] P. Wei, O. Hileman, M.-R. Bateni, X. Deng, A. Petric, Manganese deposition without additives, Surf. Coat. Technol. 201 (2007) 7739–7745.
[3] J. Cheng, B. Liu, Y. Wu, Y. Zheng, Comparative in vitro study on pure metals (Fe, Mn, Mg, Zn and W) as biodegradable metals, J. Mater. Sci. Technol. 29 (7) (2013) 619–627.
[4] J. Hufenbach, H. Wendrock, F. Kochta, U. Kühn, A. Gebert, Novel biodegradable Fe-Mn-C-S alloy with superior mechanical and corrosion properties, Mater. Lett. 186 (2017) 330–333.
[5] Y.Z.B. Liu, Effects of alloying elements (Mn, Co, Al, W, Sn, B, C and S) on biodegradability
and in vitro biocompatibility of pure iron, Acta Biomater. 7 (2011) 1407–1420.

[6] S.K. Kang, S.W. Hwang, S. Yu, J.H. Seo, E.A. Corbin, J. Shin, D.S. Wie, R. Bashir, Z. Ma, J.A. Rogers, Biodegradable thin metal foils and spin-on glass materials for transient electronics, Adv. Funct. Mater. 25 (2015) 1789–1797.
[7] B. Messaoudi, S. Joiret, M. Keddam, H. Takenouti, Anodic behaviour of manganese in alkaline medium, Electrochim. Acta 46 (2001) 2487–2498.
[8] J. Lu, D. Dreisinger, T. Glück, Manganese electrodeposition — a literature review, Hydrometallurgy 141 (2014) 105–116.
[9] L. Ding, X. Fan, J. Du, Z. Liu, C. Tao, Influence of three N-based auxiliary additives during the electrodeposition of manganese, Int. J. Miner. Process. 130 (2014) 34–41.
[10] P. Díaz-Arista, R. Antaño-López, Y. Meas, R. Ortega, E. Chainet, P. Ozil, G. Trejo, EQCM study of the electrodeposition of manganese in the presence of ammonium thyociante in chloride-based acidic solutions, Electrochim. Acta 51 (2006) 4393–4404.
[11] S.K. Padhy, P. Patnaik, B. Thipathy, I. Bhattacharya, Microstructural aspects of manganese metal during its electrodeposition from sulphate solutions in the presence of quaternary amines, Mater. Sci. Eng. B 193 (2015) 83–90.
[12] J. Lewis, P. Scaife, D. Swinkels, Electrolytic manganese metal from chloride electrolytes.
I. Study of deposition conditions, J. Appl. Electrochem. (1976) 199–209.
[13] J. Lewis, P. Scaife, D. Swinkels, Electrolytic manganese metal from chloride electrolytes.
II. Effect of additives, J. Appl. Electrochem. 6 (1976) 453–462.
[14] J. Lipkowski, Z. Galus, Electrode kinetics in mixed solvents investigations of the kinetics and equilibrium properties of manganese (II)-ammonia complexes in water and mixed solvents of n-propanol, isopropanol, t-butanol and water, Electroanal. Chem. Interfacial Electrochem. 48 (1973) 337–352.
[15] J. Gong, I. Zana, G. Zangari, Electrochemical synthesis of crystalline and amorphous
manganese coatings, J. Mater. Sci. Lett. 20 (2001) 1921–1923.
[16] C. Karwas, T. Hepel, Influence of boric acid on electrodeposition and stripping of Ni-Zn alloys, J. Electrochem. Soc. 135 (4) (1988) 839–844.
[17] J. Horkans, On the role of buffers and anions in NiFe electrodeposition, J. Electrochem. Soc. 126 (11) (1979) 1861–1867.
[18] N. Zech, D. Landolt, The influence of boric acid and sulfate ions on the hydrogen formation in Ni-Fe plating electrolytes, Electrochim. Acta 45 (2000) 3461–3471.
[19] J.M. Lee, K.K. Jung, J.S. Ko, Formation of nickel microcones by using an electrodeposition
solution containing H_3BO_3, Curr. Appl. Phys. 16 (2016) 261–266.
[20] C.H. Hamann, A. Hamnett, W. Vielstich, Electrochemistry, WILEY-VCH, Weinheim, 2007, p. 320.
[21] Echa-candidate-list-table, European Chemicals Agency, 2010 Available: https://echa.europa.eu/candidate-list-table/-/dislist/details/0b0236e1807d9b69.
[22] V. Hoffmann, R. Dorka, L. Wilken, V.-D. Hodoroaba, K. Wetzig, Present possibilities of thin-layer analysis by GD-OES, Surf. Interface Anal. 35 (2003) 575–582.
[23] S. Oswald, V. Hoffmann, Contributions to computer-aided interpretation of ion sputtering depth profiling, Spectrochim. Acta 49B (1994) 1123–1145.
[24] W. Oelßner, F. Berthold, U. Guth, The iR drop – well-know but often underestimated
in electrochemical polarization measurements and corrosion testing,

Mater. Corros. 57 (2006) 455–466.
[25] M. Chigane, M. Ishikawa, Manganese oxide thin film preparation by potentiostatic electrolyses and electrochromism, J. Electrochem. Soc. 147 (6) (2000) 2246–2251.
[26] E.I. Ilton, J.E. Post, P.J. Heaney, F.T. Ling, S.N. Kerisit, XPS determination of Mn oxidation states in Mn (hydr)oxides, Appl. Surf. Sci. 366 (2016) 475–485.
[27] M. Oku, K. Hirokawa, S. Ikeda, X-ray photoelectron spectroscopy of manganeseoxygen
systems, J. Electron Spectrosc. Relat. Phenom. 7 (1975) 465–473.
[28] X.-F. Luo, J. Wang, Z.-S. Liang, S.-Z. Chen, Z.-L. Liu, C.-W. Xu, Manganese oxide with different morphology as efficient electrocatalyst for oxygen evolution reaction, Int. J. Hydrog. Energy 42 (2017) 7151–7157.
[29] A.J. Bradley, J. Thewlis, The crystal structure of alpha-Manganese, Proc. R. Soc. A 15 (1927) 456–471.